AD

TECHNICAL REPORT ARCCB-TR-96016

ULTRASONIC AND HARDNESS STUDY OF LOW CONTRACTILE CHROMIUM DEPOSITED IN THE FLOW-THROUGH VESSEL PLATING FACILITY

STEPHAN C. SCHROEDER
JOSEPH F. COX
JOHN ASKEW
JULIUS FRANKEL
AGOSTINO ABBATE

JUNE 1996

US ARMY ARMAMENT RESEARCH,
DEVELOPMENT AND ENGINEERING CENTER
CLOSE COMBAT ARMAMENTS CENTER
BENÉT LABORATORIES
WATERVLIET, N.Y. 12189-4050

APPROVED FOR PUBLIC RELEASE; DISTRIBUTION UNLIMITED

19960828 019

DISCLAIMER NOTICE

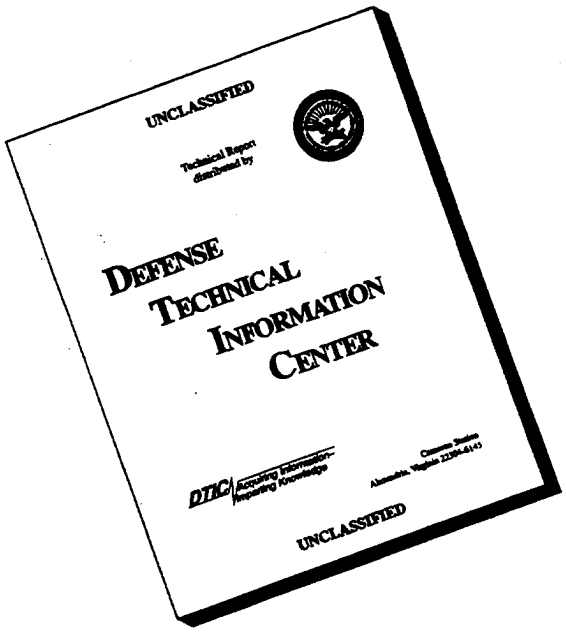

THIS DOCUMENT IS BEST QUALITY AVAILABLE. THE COPY FURNISHED TO DTIC CONTAINED A SIGNIFICANT NUMBER OF PAGES WHICH DO NOT REPRODUCE LEGIBLY.

DISCLAIMER

The findings in this report are not to be construed as an official Department of the Army position unless so designated by other authorized documents.

The use of trade name(s) and/or manufacturer(s) does not constitute an official indorsement or approval.

DESTRUCTION NOTICE

For classified documents, follow the procedures in DoD 5200.22-M, Industrial Security Manual, Section II-19 or DoD 5200.1-R, Information Security Program Regulation, Chapter IX.

For unclassified, limited documents, destroy by any method that will prevent disclosure of contents or reconstruction of the document.

For unclassified, unlimited documents, destroy when the report is no longer needed. Do not return it to the originator.

REPORT DOCUMENTATION PAGE

Form Approved
OMB No. 0704-0188

Public reporting burden for this collection of information is estimated to average 1 hour per response, including the time for reviewing instructions, searching existing data sources, gathering and maintaining the data needed, and completing and reviewing the collection of information. Send comments regarding this burden estimate or any other aspect of this collection of information, including suggestions for reducing this burden, to Washington Headquarters Services, Directorate for Information Operations and Reports, 1215 Jefferson Davis Highway, Suite 1204, Arlington, VA 22202-4302, and to the Office of Management and Budget, Paperwork Reduction Project (0704-0188) Washington, DC 20503

1. AGENCY USE ONLY (Leave blank)	2. REPORT DATE	3. REPORT TYPE AND DATES COVERED
	June 1996	Final

4. TITLE AND SUBTITLE
ULTRASONIC AND HARDNESS STUDY OF LOW CONTRACTILE CHROMIUM DEPOSITED IN THE FLOW-THROUGH VESSEL PLATING FACILITY

5. FUNDING NUMBERS
AMCMS No. 6226.24.H180.0
PRON No. J53JAT49M71A

6. AUTHOR(S)
Stephan C. Schroeder, Joseph F. Cox, John Askew,
Julius Frankel, and Agostino Abbate

7. PERFORMING ORGANIZATION NAME(S) AND ADDRESS(ES)
U.S. Army ARDEC
Benet Laboratories, AMSTA-AR-CCB-O
Watervliet, NY 12189-4050

8. PERFORMING ORGANIZATION REPORT NUMBER
ARCCB-TR-96016

9. SPONSORING / MONITORING AGENCY NAME(S) AND ADDRESS(ES)
U.S. Army ARDEC
Close Combat Armaments Center
Picatinny Arsenal, NJ 07806-5000

10. SPONSORING / MONITORING AGENCY REPORT NUMBER

11. SUPPLEMENTARY NOTES

12a. DISTRIBUTION / AVAILABILITY STATEMENT
Approved for public release; distribution unlimited.

12b. DISTRIBUTION CODE

13. ABSTRACT *(Maximum 200 words)*

The elastic properties and the yield strength of electrodeposited chromium are among the properties that determine its usefulness in corrosion and erosion protection as a coating in gun tubes. The determination of elastic properties of electrodeposited chromium, through careful measurement of ultrasonic velocities, is the main subject of this report. The elastic properties are also correlated with the coating Knoop hardness as a function of plating process parameters (current density and electrolyte flow rate). These studies can lead to a better understanding of the mechanisms involved in the deposition by observing how changes in process parameters influence the properties of the electrodeposited coating.

14. SUBJECT TERMS	15. NUMBER OF PAGES
Elastic Properties, Ultrasonics, Chromium, Hardness, Coatings, Electrodeposition	30
	16. PRICE CODE

17. SECURITY CLASSIFICATION OF REPORT	18. SECURITY CLASSIFICATION OF THIS PAGE	19. SECURITY CLASSIFICATION OF ABSTRACT	20. LIMITATION OF ABSTRACT
UNCLASSIFIED	UNCLASSIFIED	UNCLASSIFIED	UL

TABLE OF CONTENTS

Page

ACKNOWLEDGEMENTS iii

INTRODUCTION 1

EXPERIMENTAL PROCEDURE 2

Sample Preparation 2

Mechanical Measurements 3

Ultrasonic Measurements 3

Etching of Chromium 4

Metallography and Microhardness Measurements 4

NONDESTRUCTIVE DETERMINATION OF ELASTIC CONSTANTS USING ULTRASONICS 5

EXPERIMENTAL RESULTS 6

Hardness Data 8

ERROR ANALYSIS OF VELOCITY MEASUREMENTS 9

DISCUSSION 10

CONCLUSIONS 12

REFERENCES 13

TABLES

1. Measured and Calculated Working Elastic Properties 7

LIST OF ILLUSTRATIONS

1. Schematic showing the cylindrical section of a 120-mm barrel showing lines used for alignment during thickness measurements at four locations 14

DTIC QUALITY INSPECTED 3

2. The measured transverse sound velocity of the chromium plotted as a function of normalized current density for two flow rates 15

3. The measured transverse sound velocity of the steel plotted as a function of normalized current density for two flow rates 16

4. The measured longitudinal sound velocity of the chromium plotted as a function of normalized current density for two flow rates 17

5. The measured longitudinal sound velocity of the steel plotted as a function of normalized current density for two flow rates 18

6. The calculated value of the Young's modulus of the chromium plotted as a function of normalized current density for two flow rates 19

7. The calculated value of the Young's modulus of the steel plotted as a function of normalized current density for two flow rates 20

8. The calculated value of the shear modulus of the chromium plotted as a function of normalized current density for two flow rates 21

9. The calculated value of the shear modulus of the steel plotted as a function of normalized current density for two flow rates 22

10. The calculated value of the bulk modulus of the chromium plotted as a function of normalized current density for two flow rates 23

11. The calculated value of the bulk modulus of the steel plotted as a function of normalized current density for two flow rates 24

12. The calculated value of the Poisson's ratio of the chromium plotted as a function of normalized current density for two flow rates 25

13. The calculated value of the Poisson's ratio of the steel plotted as a function of normalized current density for two flow rates 26

14. Knoop hardness data on chromium obtained in the present report in the shop VPF using the flow-through method at flow rate of R1 and R2 and for plates done in the laboratory in beakers from reports by Chen and Pan et al., all plotted as a function of normalized current density 27

ACKNOWLEDGEMENTS

We are pleased to acknowledge with gratitude the advice of Dr E. S. Chen, the untiring help and plating expertise of Mr. F. Nelson, and the competence of Mr. C. Rickard in performing the Knoop hardness measurements and chromium metallographic examination.

INTRODUCTION

The demands placed on the coatings under study are the most severe imaginable. Pressure pulses of over 100,000 psi and temperature pulses in excess of 1800°F superposed on the mechanical effects of internal stresses, chemical effects of the combustion byproducts, and on the mechanical forces of the projectile or rotating bands compete to erode, melt, crack, flake, and deform the chromium coatings that are often about 0.005 inch thick.

Until now, high contractile chromium (HCC) has been used for this application. Now, low contractile chromium (LCC) is being plated and tested for improved bore protection. Unlike HCC, LCC does not "precrack" on plating, it is softer, and it has superior adherence to the steel substrate. One study, however, showed more flattening of GAU-8/A lands coated with LCC, presumably because of the lower hardness of the LCC deposit (ref 1). Other differences between the two coating types, which are prepared using different solution temperatures (140°F for HCC and 180°F for LCC) and different current densities (that of HCC ≅0.3 LCC), will be discussed later.

Low contractile chromium is deposited in the Vessel Plating Facility (VPF) at the Watervliet Arsenal. The first work here has been done by Dr. E.S. Chen and collaborators (refs 2,3) on the deposition and evaluation of LCC coatings for laboratory scale specimens. Others have done follow-up work.

What we present here are the first measurements of the elastic properties of LCC coatings, along with Knoop hardness measurements on the same specimens. All coatings were deposited in the VPF on 2-foot long, 120-mm bore sections with a wall thickness of 0.8 inch. In order to study and eventually optimize the effectiveness of the LCC deposition process, the available process parameters, current density, and flow rate of the plating solution were varied and measurements were made on the resulting coatings. Nine separate sections were plated at flow rates of 460 and 550 gpm and current densities from 90 to 250 amps/dm^2.

Ultrasonic techniques were used to measure the elastic properties of the LCC coatings at 28 spots located along 4 lines on each ring. The small thickness of the chromium coating (0.005 to 0.01 inch) and the small difference in acoustic impedance between the steel substrate and the chromium coating (~4.2 percent with a reflection coefficient of 0.02), forbade routine direct bulk velocity measurements to obtain chromium elastic properties. We obtained all of our data by a difference technique, measuring return times and specimen wall thicknesses before and after the chromium deposits were etched from the surface of the steel substrate and dividing the change in thickness by the change in return time to obtain velocities. All property determinations were made at room temperature, but the coatings are used at high temperatures; hence this work can best be considered the beginning of efforts to use nondestructive testing techniques to understand and predict the ability of LCC coatings to protect the steel bore.

Up until now, no fundamental understanding or mechanistic model has existed as to why or how LCC instead of HCC chromium gets deposited. Because of the complexity of the processes involved, the effect of various plating parameters is not understood, although empirical plating procedures have been developed. We know, from previous work, that plating solution temperature and current density are important factors in determining the nature of electrodeposited chromium. In the work described here, solution temperature was fixed for all depositions, and the effect of the current density on deposit properties was determined. In addition, the possible influence of solution flow rate on deposit properties was evaluated.

There is an indication by some (ref 4) that the [211] crystallographic direction is predominant in LCC; others (ref 5) have reported no pronounced orientation for LCC deposits and a very pronounced [111] orientation for HCC. Preferred [111] orientation of HCC is confirmed in many reports (refs 6,7). The microstructures of the two deposits are different. HCC has a thin stringy, cracked structure whereas LCC seems to grow in a finger-like, sometimes feathered morphology where growth is also in the electric field direction. LCC is softer than HCC and does not exhibit the network of microcracks that is characteristic of HCC. Also when the two forms of chromium are heated to about 1350°F and then returned to room temperature, HCC shows a large permanent contraction, while LCC shows little if any dimensional changes. The large shrinkage of HCC is thought to be due to the decomposition, at high temperature, of codeposited impurities.

Our measurements add new features to the quest for obtaining greater insight into the properties of plated chromium:

1. We report on spot-by-spot elastic property determinations on LCC produced in shop facilities by measuring longitudinal and shear sound waves whose propagation is in the deposition direction; i.e., we obtain elastic constants in the deposition direction.

2. We provide Knoop hardness measurements made on samples obtained from the same tubes, but in a direction perpendicular to the growth direction.

3. We integrate data from previous work in order to view our measurements in a larger context.

EXPERIMENTAL PROCEDURE

Sample Preparation

Low contractile chromium was plated on large caliber tube sections by means of the flow-through technique. Here the bore of the tube contains the plating solution, which is pumped in from the bottom at a constant flow rate and temperature. The anode is a solid, lead-plated cylinder concentric with the bore. The inside of the tube is thus plated with chromium. Nine

tubes were plated in the VPF using the flow-through plating process at specific flow rates and current densities for each tube. Hydrogen was removed from the chromium plated cylinders by heating at 560°F for 5 hours.

Rings 1.675 inches in height (Figure 1) were cut from each of the nine tubes. The rings had an outside diameter (OD) of 6.33 inches and an inside diameter (ID) of 4.72 inches (i.e., a wall thickness of about 0.80 inch). The flat faces of each ring were machined parallel to one another. Straight lines not visible in the figure, perpendicular to the parallel faces, were drawn on the inner surface at 90° intervals around the inner diameter of each ring. Each line was continued on the flat face as a straight line that was perpendicular to both the bore surface and the exterior surface of the ring. These lines, visible in the figure, were used as positioning marks for measurements of chromium thickness by use of a dial indicator.

Mechanical Measurements

The wall thickness at each of the four ring positions, before and after removal of the chromium electrodeposit, was determined by placing the ring with its outer surface on a flat granite plate so that one of the lines drawn on a flat face was perpendicular to the granite plate. A dial indicator and a Cadillac® gauge, with a combined resolution of two-hundred-thousandths of an inch ($2x10^{-5}$ inches), were used to measure ring wall thickness at seven points, at one-quarter inch intervals along one of the four lines that had been drawn on the bore surface. Each point on the line was measured mechanically three times to get an average wall thickness and also to determine the reproducibility of the thickness measurements. Wall thickness was determined along each of the four lines drawn on the bore surfaces of the nine ring specimens.

Ultrasonic Measurements

The ultrasonic pulse-echo technique uses an oscilloscope, an electronic signal generator, an electronic clock, a signal amplifier, and both a shear and longitudinal ultrasonic transducer. A pulse-echo system with a single-element transducer operates as follows: at a regular interval, the electronic clock triggers the signal generator to send a short pulse of high-frequency alternating voltage to the transducer. Simultaneously, the clock activates a time-measuring circuit, which is connected to the oscilloscope. The transducer element converts the voltage pulse into a pulse of mechanical vibration replicating in large part the frequency and amplitude characteristics of the imposed voltage. This mechanical vibration (ultrasound) is transferred into the workpiece through a couplant and travels by wave motion through the piece. This wave travels at the speed of sound of the material. When this ultrasonic pulse encounters a reflecting surface perpendicular to the direction of travel, the ultrasonic energy is reflected back toward the transducer. This returning pulse travels at the same speed and along the same path as the transmitted wave except in the opposite direction. The arrival of the returning pulse at the transducer causes it to vibrate; this, in turn, induces an alternating electrical voltage across the transducer. The voltage is amplified and then fed into the measuring electronics. This process of alternately sending and

receiving pulses of ultrasonic energy is repeated for each successive pulse. The time for the ultrasonic pulse to make one round trip through the ring wall is recorded and measured to a resolution of better than one nanosecond ($1x10^{-9}$ sec). To insure that the transducer is in intimate contact with the surface, a Quick-grip® clamp is used to secure the transducer to the surface of the ring. All of the time and thickness measurements are made at room temperature (65 to 70°F).

Ultrasonic measurements were made using one-quarter inch diameter, 5 MHZ, shear or longitudinal, commercially available, piezoelectric transducers. Measurements were made before and after chromium was removed from bore surfaces, at seven spots along each of the four lines drawn on the bore surface of each ring (112 ultrasonic measurements for each ring). Spot-check measurements of shear velocities with shear polarization parallel and perpendicular to the tube axis yielded the same values.

Etching of Chromium

After the wall thicknesses and echo return times along each line were measured, chromium was removed from the bore surface of each ring specimen using a chromium stripping solution. The ring was masked with an insulating coating to ensure that only chromium one-half inch on either side of the line was removed. The etching solution consisted of 265 gm of acetic acid, 440 gm of demineralized water, and 3300 gm of 85 weight percent orthophosphoric acid. The steel ring was the anode. A copper sheet cathode was placed about a quarter inch away from the chromium surface to be etched. The cathode-to-anode surface area ratio was about two. The ring was placed in the solution which was heated to about 35°C, and continuously stirred so that the solution between the cathode and the anode did not become concentrated with stripped chromium. The current was increased until bubbling action at the anode was seen. It was kept constant until all of the chromium was stripped. Typical values for the current and applied voltage were 3 amps and 7.5 volts, respectively. After all of the chromium was stripped, the insulating coating was removed and the ring was cleaned with water. Chromium was removed at a greater rate at all edges (where current densities are greatest) so that the last chromium to be removed was a small island in the center of the region being stripped. Very little steel was removed during the stripping, but even so data used for the analysis were obtained only from those portions of the ring that were in or near the center of each stripped area and that showed no steel loss.

Metallography and Microhardness Measurements

Samples from each tube were subjected to metallographic examination. Cross-sectional samples of each ring were etched with Murakami's reagent (10 gm K_3 $Fe(CN)_6$, 10 gm NaOH in 10 ml of H_2O) in order to reveal the microstructure and crack characteristics of the chromium electrodeposited with each set of process parameters. The high density of microcracks, characteristic of HCC deposits, was not found in any of the coatings. Some of the specimens showed evidence of machining marks in the steel, one-thousandth of an inch (0.001 inch) deep.

Metallographic examination of the samples did show that the surface roughness of deposits was associated with very rough surfaces of the steel substrate. As a result of this roughness, actual variations in thickness of some chromium deposits were not accounted for by our reproducible but averaging (over the dial indicator tip) thickness-measuring technique.

The microhardness on the cross-sectional faces of electrodeposited chromium was determined, before the samples were etched, using a Knoop indenter with a 50-gm applied load.

NONDESTRUCTIVE DETERMINATION OF ELASTIC CONSTANTS USING ULTRASONICS

Using the wall thicknesses and the pulse-echo return times for the ring before and after the removal of the chromium, the shear and longitudinal speed of sound was determined using the following equations:

$$V_{Steel}=2\frac{X_{Steel}}{\Delta t_{Steel}} \tag{1}$$

$$V_{Chromium}=\frac{2(X_{Total}-X_{Steel})}{\Delta t_{Total}-\Delta t_{Steel}} \tag{2}$$

where

V_{chrome}	=	Velocity of sound in electroplated chromium
V_{steel}	=	Velocity of sound in steel
X_{total}	=	Wall thickness measured before etching
X_{steel}	=	Wall thickness measured after etching
Δt_{Total}	=	Ultrasonic return time measured before etching
Δt_{Steel}	=	Ultrasonic return time measured after etching

Using Eqs. (1) and (2), the speed of sound was calculated for steel and chromium for both the shear and longitudinal modes, where the propagation direction of the pulses was in the direction normal to the plate surface. These speeds of sound will be used in Eqs. (3) through (6).

An isotropic material requires only the two Lamè constants λ and μ in order to yield a complete description of the elastic properties. As we stated, electrodeposited LCC has been found to have some anisotropy. The symmetry axis has been found to be in the direction of growth, which is mostly in the direction normal to the plate surface. At this time not enough information regarding the degree and crystallographic orientation or anisotropy for our specimens is available to incorporate the data in an anisotropy calculation. Further, as will be seen later, the

variability of the sound velocity is up to 12.4 percent (much higher than would be expected from our measurement errors) for one value of the current density, so that even though isotropic conditions do not exactly apply, the variability of the velocities and the novelty of the data justify our presentation of elastic properties such as Young's modulus, shear modulus, bulk modulus, and Poisson's ratio as approximate values and the best available working data to date.

The following equations, based on the assumption of isotropic properties, were used to calculate the working elastic quantities:

$$E = 3V_S^2\rho\frac{\left(V_L^2 - \frac{4}{3}V_S^2\right)}{V_L^2 - V_S^2} \tag{3}$$

$$\nu = \frac{V_L^2 - 2V_S^2}{2\left(V_L^2 - V_S^2\right)} \tag{4}$$

$$G = \rho V_S^2 \tag{5}$$

$$B = \rho\left(V_L^2 - \frac{4}{3}V_S^2\right) \tag{6}$$

where

V_S	=	Speed of sound for shear waves
V_L	=	Speed of sound for longitudinal waves
ρ	=	Density of the material being measured
ν	=	Poisson's ratio

EXPERIMENTAL RESULTS

From mechanical measurements of steel and chromium thicknesses and the time of flight measured using ultrasonic techniques, the velocity of sound for shear and longitudinal waves was calculated for both the chromium and the steel sections using Eqs. (1) and (2). The average speed of sound along with its standard deviation for steel and chromium was calculated for each of the four lines on the sample. From the average speed of sound for both the shear and longitudinal

waves, using the assumption of isotropy, the working Young's modulus, Poisson's ratio, bulk modulus, and shear modulus were calculated using Eqs. (3) through (6) (See Table 1). The density (ref 4) of electroplated chromium was taken as 7200 kg/m^3 and the density of 4340 steel was 7840 kg/m^3.

Table 1. Measured and Calculated Working Elastic Properties

	Shear Velocity (m/sec)	Longitudinal Velocity (m/sec)	Young's Modulus (GPa)	Poisson's Ratio	Shear Modulus (GPa)	Bulk Modulus (GPa)	Knoop Hardness
Steel	3230 ± 2	5910 ± 4	210 ± 0.4	0.287 ± 0.0004	82 ± 0.2	165 ± 0.4	
Sample #1	3323 ± 140	6447 ± 378	209 ± 16	0.316 ± 0.032	80 ± 7	194 ± 35	609.45
Sample #2	3820 ± 200	6706 ± 535	265 ± 31	0.255 ± 0.038	105 ± 11	185 ± 37	772.55
Sample #3	3300 ± 297	5738 ± 456	197 ± 33	0.249 ± 0.044	79 ± 14	133 ± 27	551.48
Sample #4	3854 ± 127	7159 ± 476	277 ± 20	0.291 ± 0.033	107 ± 7	228 ± 45	764.98
Sample #5	3563 ± 222	5941 ± 739	221 ± 33	0.201 ± 0.076	92 ± 11	136 ± 57	639.90
Sample #6	3670 ± 231	6273 ± 427	240 ± 29	0.234 ± 0.051	97 ± 12	155 ± 31	673.75
Sample #7	3415 ± 275	5875 ± 285	209 ± 29	0.243 ± 0.035	85 ± 14	136 ± 12	644.78
Sample #8	3757 ± 317	6134 ± 517	244 ± 41	0.196 ± 0.040	102 ± 18	136 ± 29	732.93
Sample #8	3757 ± 317	6143 ± 407	234 ± 29	0.226 ± 0.045	95 ± 13	146 ± 29	626.08
Voigt	3975	6653	283	0.209	117	162	
Reuss	3953	6635	280	0.212	115	162	
Hashin	3950	6633	279	0.212	115	162	
Shtrikman	3929	6616	277	0.215	114	162	

Table 1 also gives the expected range of values of the elastic properties. These were calculated from the elastic stiffnesses (C_{ij}) and the elastic compliances (S_{ij}) of single-crystal data using Voigt and Reuss methods, respectively. It was shown that these average values were the least upper bound (Voigt) and the greatest lower bound (Reuss) for the elastic velocities. Hashin and Shtrikman developed expressions that narrowed the Voigt and Reuss bounds for aggregates of cubic crystals (ref 8). They found that the difference between the bounds was at least a factor of two smaller for most materials. All of the single-crystal chromium data and the aforementioned derived values are found in Reference 8.

Figures 2 through 5 show the shear and longitudinal velocities of sound in both chromium and steel as functions of current density. The velocity of sound in the steel ring was found to be independent of current density used for chromium plating. The average longitudinal and shear velocities in steel were determined to be 5910 ±4 m/sec and 3230 ±2 m/sec, respectively. The estimated average velocity of sound in the chromium deposits increased by about 20 percent over the range of current density.

Figures 6 and 7 show Young's moduli of chromium and steel as functions of current density. The average Young's modulus for steel was determined to be 210 ±0.4 GPa and was independent of current density. The average estimated Young's modulus for chromium increased monotonically by roughly 25 percent for our current density range.

Figures 8 and 9 depict shear moduli of both chromium and steel as functions of current density. The shear modulus for steel is independent of current density and has an average value of 82 ±0.2 GPa. The average estimated shear modulus for chromium increased monotonically by about 25 percent for our current density range.

Figures 10 and 11 plot the bulk moduli of chromium and steel as functions of current density. An average bulk modulus for steel of 165 ±0.4 GPa, independent of current density, was obtained. The average estimated bulk modulus of chromium increased by roughly 40 percent with increasing current density.

Figures 12 and 13 show Poisson's ratio for chromium and steel as functions of current density. Poisson's ratio for steel is independent of current density and has an average value of 0.287 ±0.0004. Poisson's ratio for chromium showed roughly no increase with increasing current density, but the scatter in the measured values was large.

Values for the three moduli and Poisson's ratio, calculated from single-crystal data, are given in Table 1, and are shown in the appropriate columns as the values obtained by the Hashim-Shtrikman methods.

Hardness Data

Figure 14 shows a comparison of the dependence of Knoop hardness on current density for chromium prepared in the shop VPF, and for data obtained by Chen (ref 3), and by Pan et al. (ref 4), from chromium electrodeposited onto the external surfaces of one-quarter inch diameter copper and brass cylinders. Pan et al. used a rotating cylindrical cathode with a flat platinum anode to prepare LCC, while Chen used rotating cylindrical cathodes with a lead sheet concave anode, placed to have symmetrical electric fields on the sample. The weight ratio of CrO_3 (chromic anhydride) to sulfuric acid is 100:1 for all these experiments. The other experimenters obtained data over a smaller range of reported current densities, but still well within the upper and lower bounds used in our experiments. Our data show a monotonic relationship between hardness and current density with a positive but very slowly decreasing slope. Results reported by Chen agree with the present data, but the results of Pan et al. do not agree with the results of either study.

ERROR ANALYSIS OF VELOCITY MEASUREMENTS

The scatter in measured velocities observed in the experimental results is indicative of both the error in the measurements and the spatial variation of sound velocity in the sample. In order to separate these contributions, an error analysis of the measurements was conducted. Errors in the measurement are due to scatter of time and thickness readings due to noise or other uncertainty.

One standard deviation for measurement of sample thickness is $\varepsilon_X = 1 \times 10^{-4}$ inches and for determination of time-of-flight values, it is $\varepsilon_{\Delta t} = 1 \times 10^{-9}$ seconds. To calculate the total error associated with the velocity estimation, the following reasoning is used (ref 9). In general, for the equation $y = f(x_1, x_2)$, one standard deviation ,ε_y, for the measurement is calculated as

$$\varepsilon_y = \sqrt{\left(\frac{\partial y}{\partial x_1}\right)^2 \varepsilon_{x_1}^{\,2} + \left(\frac{\partial y}{\partial x_2}\right)^2 \varepsilon_{x_2}^{\,2}} \tag{7}$$

Using Eq. (7), the errors in the chromium and steel velocity measurements are

$$\varepsilon_{V_{Steel}} = \sqrt{\left(\frac{2}{\Delta t_{Steel}}\right)^2 \varepsilon^2{}_X + \left(\frac{2X_{Steel}}{\Delta t^2{}_{Steel}}\right)^2 \varepsilon^2{}_{\Delta t}} \tag{8}$$

$$\varepsilon_{V_{Chrome}} = \sqrt{\frac{8}{\left(\Delta t_{Total} - \Delta t_{Steel}\right)^2} \varepsilon_X^2 + \frac{8\left(X_{Total} - X_{Steel}\right)^2}{\left(\Delta t_{Total} - \Delta t_{Steel}\right)^4} \varepsilon_{\Delta t}^2} \tag{9}$$

Using representative measured values for thickness and ultrasonic travel time in chromium and in steel, the errors for velocity measurements made on sample two, line three, point four, were calculated from Eqs. (8) and (9). At this location the thickness of chromium and steel was 0.00873 inch and 0.8187 inch, respectively. The time for the ultrasonic longitudinal wave traveling through the chromium and the 4340 steel was 64 nsec and 704.2 nsec, respectively. The time for the ultrasonic transverse wave traveling through the chromium and the 4340 steel was 113 nsec and 1288.8 nsec, respectively. The longitudinal velocity of sound in the chromium and

the 4340 steel was 6929 m/sec and 5905 m/sec, respectively. The error in the longitudinal chromium velocity measurement was 189.9 m/sec or a relative error of 2.7 percent, and the error in the longitudinal 4340 steel velocity measurement was 1.11 m/sec or a relative error of 0.019 percent. The transverse velocity of sound in the chromium and the 4340 steel at this point was 3925 m/sec and 3227 m/sec, respectively. The error in the transverse chromium velocity measurement was 80.3 m/sec or a relative error of 2.0 percent, and the error in the transverse 4340 steel velocity measurement was 0.47 m/sec or a relative error of 0.014 percent.

The previous discussion is based on the estimated values of ε_X and $\varepsilon_{\Delta t}$. These values were calculated using multiple readings at the same locations for the thickness measurements and signal time averaging for travel time measurements.

These values for one standard deviation for velocity measurements made at a single point represent the expected variation in velocity readings due to measurement errors, and must be compared with the variation in measured values presented in Table 1. The velocity variations reported in the table were obtained by averaging velocity measurements for each of the rings and then calculating the associated standard deviations. These variations are much greater than the errors we would expect from the above analysis, thus suggesting that the measured standard deviation in the velocities reported in Table l is most likely caused by spatial variations in material properties which cannot be accounted for at the present time. It has to be pointed out that some samples exhibited rougher surfaces, but we could not find any correlation with the results in the table.

DISCUSSION

The agreement between our hardness data and the data of Chen (ref 3) is encouraging; despite differences in plating conditions used to electrodeposit chromium samples, this is the first reported agreement between shop and laboratory data. The discrepancy with the data of Pan et al. (ref 4) cannot be explained.

Additionally, regarding the trend of measured Knoop hardness with current density, the chromium is softest at the lowest current density and increases monotonically with current density to values that are comparable to low hardness values for HCC.

Figures 3 and 5 give the values of the longitudinal and shear velocities in chromium. Again, we see what can be interpreted as monotonically increasing velocities with current density. Interestingly at the highest current density, the shear velocity is slightly lower and the longitudinal velocity is about the same as the values calculated from the single-crystal data referenced in Simmons and Wang (ref 8). Specifically, for the measured longitudinal velocity, the value for LCC at a normalized current density of 2.5 is about 6700 m/sec with a ±10 percent scatter.

Hardness empirically is directly related to the ultimate tensile strength of a material. This in turn is closely related to the yield strength, which represents the onset of "engineering" plastic deformation. The facilitators of plastic deformation in the lattice are dislocations. The movement of dislocations through the lattice is impeded when a dispersed second-phase, point defects, grain boundaries, or high dislocation densities are present. These serve to pin dislocations, hinder their glide through the lattice, and hence minimize the slip. When more defects are present, there is more dislocation pinning, and plastic deformation would require higher stresses because the dislocations would have to break away from more of these pins for further plastic deformation to occur. In our case, the dislocation movement through the lattice could be impeded by the codeposited second-phase particles, consequently plastic deformation and therefore yielding is postponed to higher stresses. This results in greater hardness. It is known that annealing HCC for a short time at 1260°F causes softening. This could be explained mainly by decomposition of the codeposited hydrated chromic oxide, but also with a smaller likelihood of annealing effects such as reduction of residual stresses, grain growth, and decreased dislocation densities. Also shrinking of the HCC specimens in thermal expansion measurements, as mentioned before, can be understood within this mechanism: the codeposited compound decomposes, hydrogen released by the decomposition escapes from the specimen, oxygen released by the decomposition reacts with chromium to form more chromium oxide, the chromium oxide agglomerates, and the specimen shrinks. The specimen also becomes softer and as noted before, the density increases.

The changes in the sound velocities with current density are harder to discuss, in view of the present lack of information on the relationship of preferred orientation change, or of concentration on codeposited species with current density, and its effect on the velocity. The features of note are that for LCC deposited at low current density, the velocities are lower and at higher current densities, the velocities are higher (monotonically increasing as a function of current density). At the highest value of the current density, the average value of the velocities is close to values calculated from single-crystal elastic constants via the Hashim-Shtrikman methods. The other extremely noteworthy feature is that the variation in the measured values ranges from 3.3 to 9 percent for transverse and 4.9 to 12.4 percent for longitudinal velocities for the same value of the current density, within a controlled experiment. The error of the measurement, as described above, for a particular case was 2 percent for transverse and 2.7 percent for longitudinal velocities.

Generally sound velocity is a function of interatomic potentials, so crystallographic orientation, phase changes, impurities, dislocation densities, and average dislocation loop lengths all affect the velocities. If we say that the codeposited second-phase causes increased average stiffness at high current densities, which then result in higher velocities, we have to match that to the empirical evidence that these velocities do not exceed the values predicted from single-crystal elastic constants. Thus the hardening mechanism with current density is superposed on a lattice that is softer at the lower current densities. This presents the need for more data, maybe in the form of preferred crystallographic orientation and its change in preponderance with current density. Both hardness and sound velocity depend on crystallographic orientation.

CONCLUSIONS

The following conclusions can be drawn from this work:

1. A correlation was found **for the first time** between hardness data obtained in the laboratory and in the shop for the deposition of LCC chromium as a function of current density.

2. Spot ultrasonic measurements were made on electrodeposited chromium. For the first time, the spatial variation of the elastic parameters was obtained for plated chromium specimens. On the basis of ultrasonic velocity measurements made at various spots in the chromium plate, spatial variations in velocities were found on one specimen of up to 12.4 percent.

3. No noticeable correlation was found in the data or the velocities as a function of flow rate in the flow-through method.

4. A direct monotonic relationship was found between sound velocities and flow rate and Knoop hardness and flow rate. The lowest values for both were found at the lowest current densities. Hence **for the first time** the means are available now to relate hardness to a non-destructive measurement, namely of the sound velocities. **Therefore the quality of the coating can now be evaluated by means of a nondestructive measurement**.

5. Working values of elastic properties in the electrodeposited chromium were found as a function of current density.

6. Metallographic examination of the specimens indicated that the crack-free features of LCC were preserved for the whole range of current densities.

REFERENCES

1. S.R. Duke, D. Perrin, and M.A. Blair, "GAU-8/A Barrel-Life Improvement Program, Microflash Photography Post-Test Metallographic Results," *Proceedings of the Tri-Service Gun Tube Wear and Erosion Symposium*, (J.P. Packard, A. Ahmad, and A. Braced, Eds.), Sponsored by ADPA and ARDEC, 1982, pp. 72-89.

2. E.S. Chen and W. Baldauf, "Improved LC Chromium for Gun Tube Application," Technical Report ARLCB-TR-80008, Benet Laboratories, Watervliet, NY, March 1980.

3. E.S. Chen, "Improved Electrodeposited Low Contractile Chromium," Technical Report ARLCB-TR-92009, Benet Laboratories, Watervliet, NY, April 1982.

4. S.K. Pan, M.D. Miller, and F.J. Nelson, "Optimization of Plating Parameters for Low Contraction Chromium Electrodeposits," Technical Report ARCCB-TR-89024, Benet Laboratories, Watervliet, NY, October 1989.

5. M.H. Kamdar and R.M. Fisher, "Structure of Electrodeposited Chromium on Gun Steel," Technical Report ARLCB-TR-85036, Benet Laboratories, Watervliet, NY, September 1985.

6. N.M. Martyak and R. Weil, "Structure Studies of Chromium Electrodeposits," *Materials Characterization*, Vol. 28, No. 2, March 1992, pp. 113-120.

7. H. Matsubayashi, W. Kurokawa, and H. Sano, "Effects of Crystallographic Orientation on the Growth of Electrodeposited Metallic Chromium," *J. Met. Finish. Soc. Japan*, Vol. 35, No. 7, July 1984, pp. 354-358.

8. G. Simmons and H. Wang, *Single Crystal Elastic Constants and Calculated Aggregate Properties, A Handbook*, The MIT Press, 1971.

9. J.P. Nickol, K.H. Moore, H.F. Meiners, and W. Eppenstein, *Analytical Laboratory Physics*, J.W. Edwards, Publisher, Inc., Ann Arbor, MI, 1956, pp. 10-44.

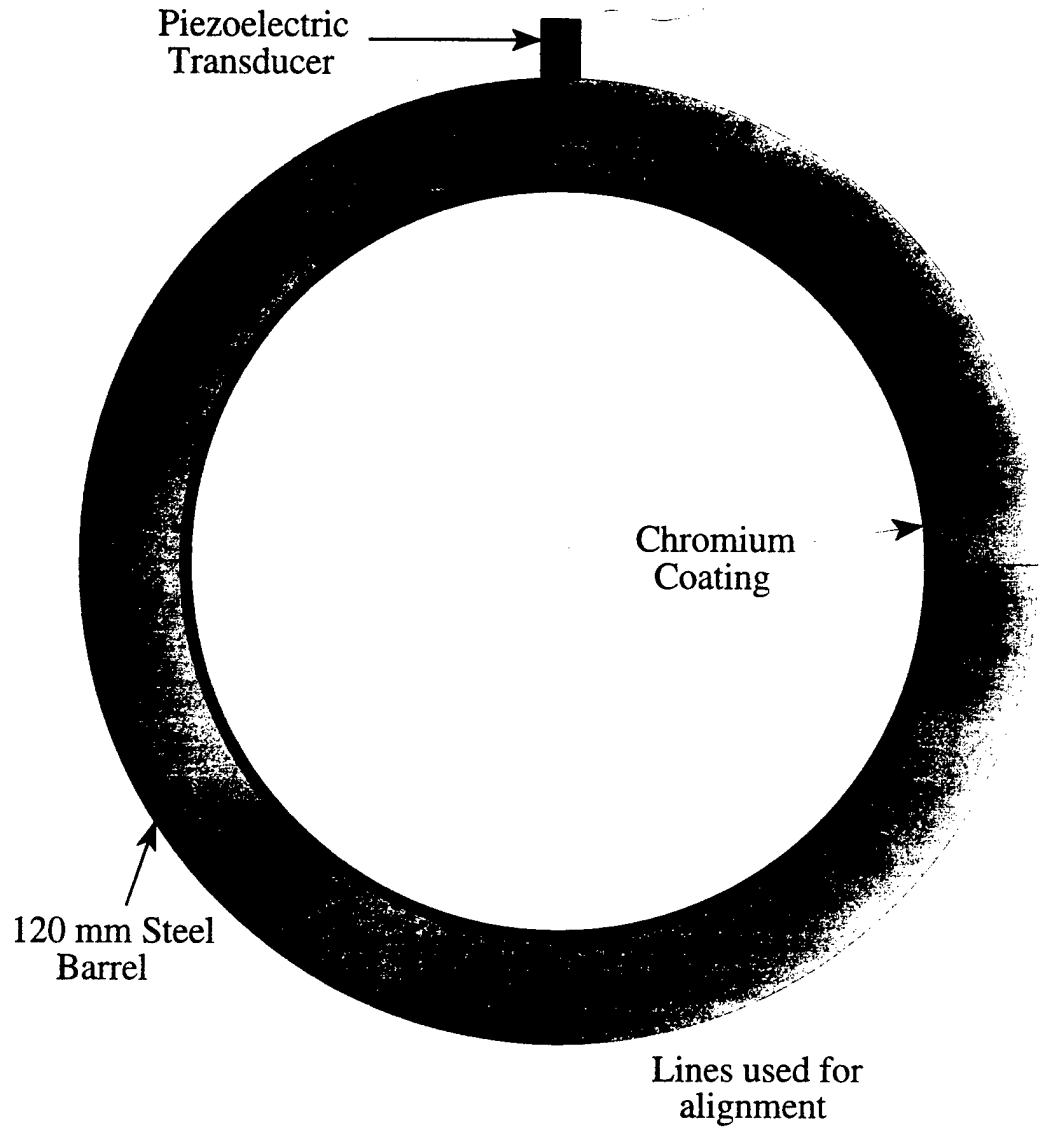

Figure 1 Schematic showing the cylindrical section of a 120 mm barrel showing lines used for alignment during thickness measurements at four locations. Thickness and time measurements were made at each of these locations before and after the chromium was removed.

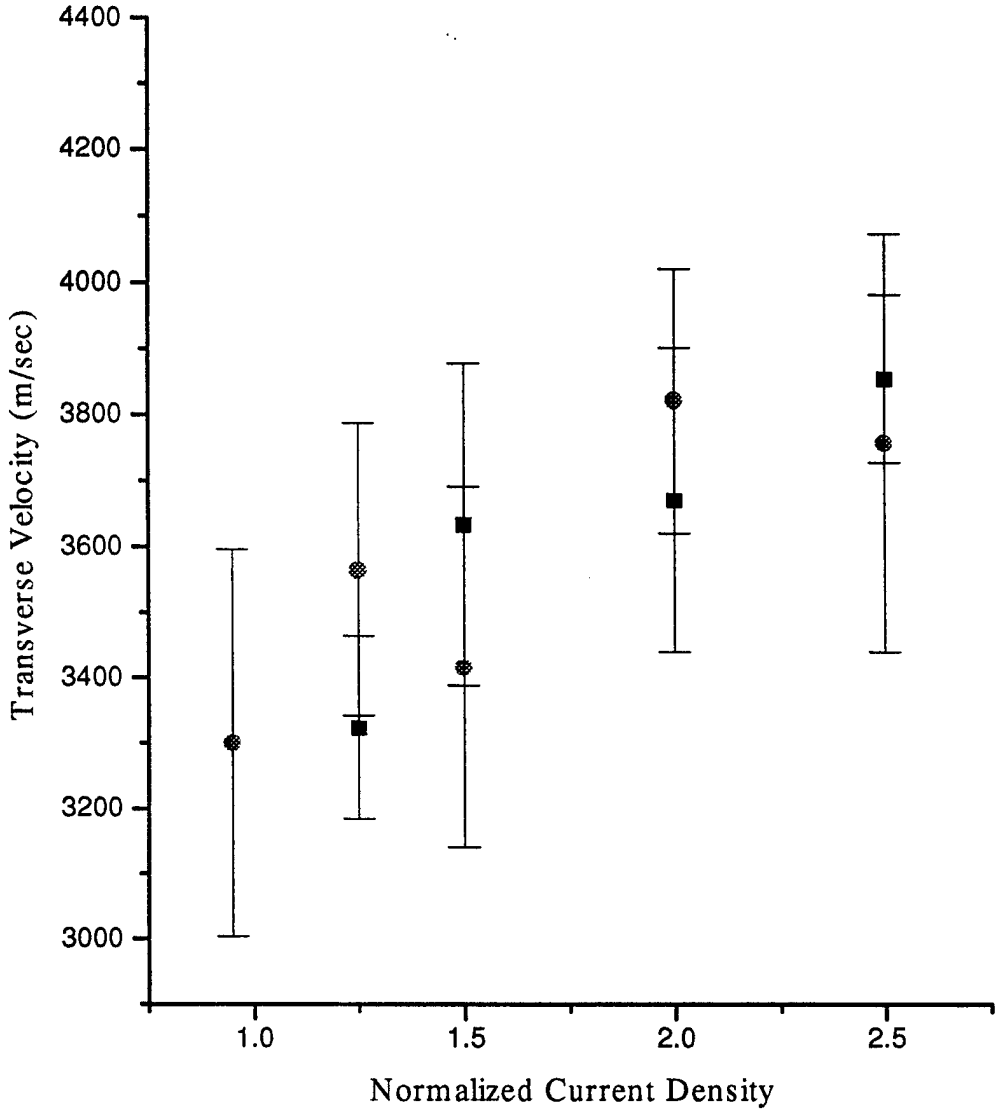

Figure 2 The measured transverse sound velocity of the chromium plotted as a function of normalized current density for two flow rates, ■ flow rate R1 and ● flow rate R2, respectively. Each point represents the average of the readings for all four locations on a ring and the bars represent the range in values for each ring.

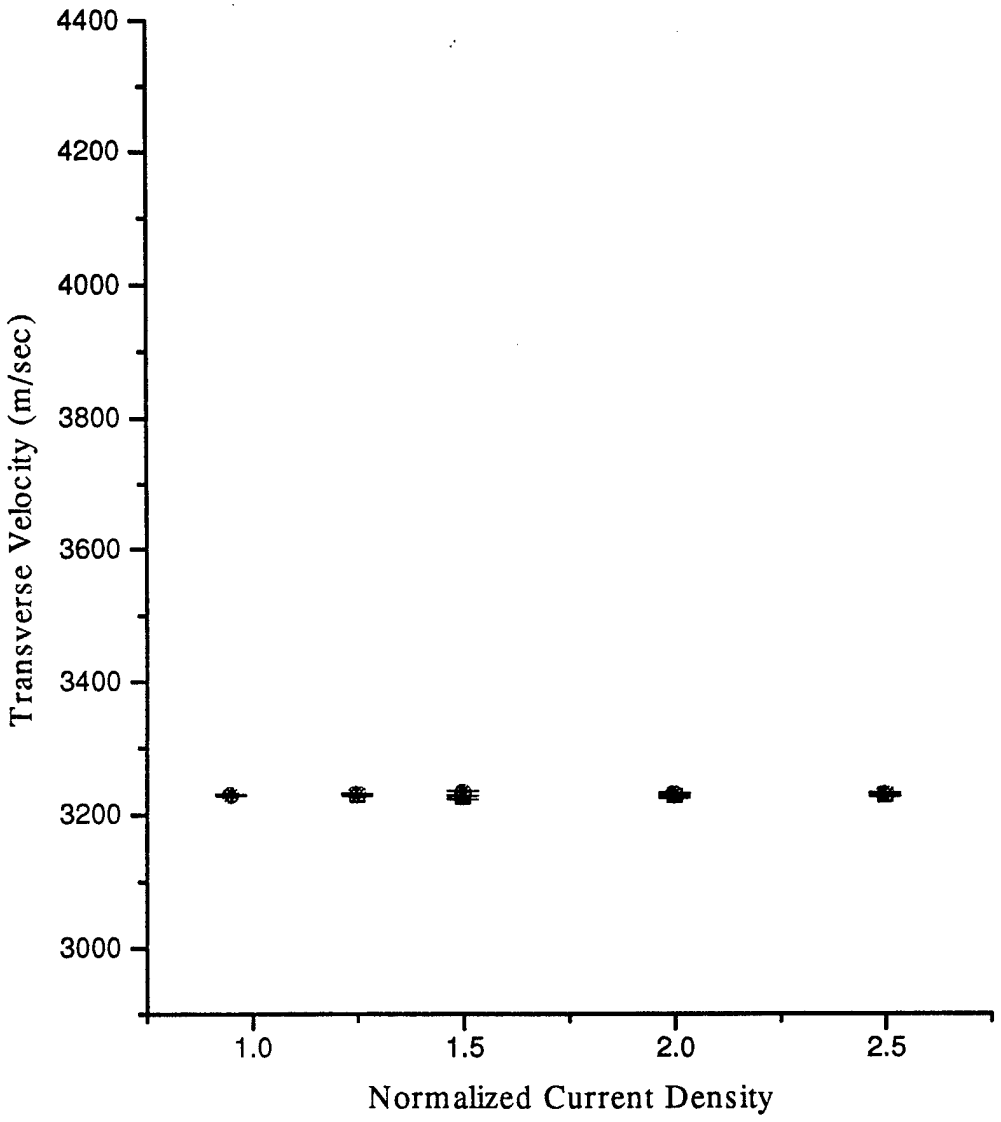

Figure 3 The measured transverse sound velocity of the steel plotted as a function of normalized current density for two flow rates, ■ flow rate R1 and ● flow rate R2, respectively. Each point represents the average of the readings for all four locations on a ring and the bars represent the range in values for each ring.

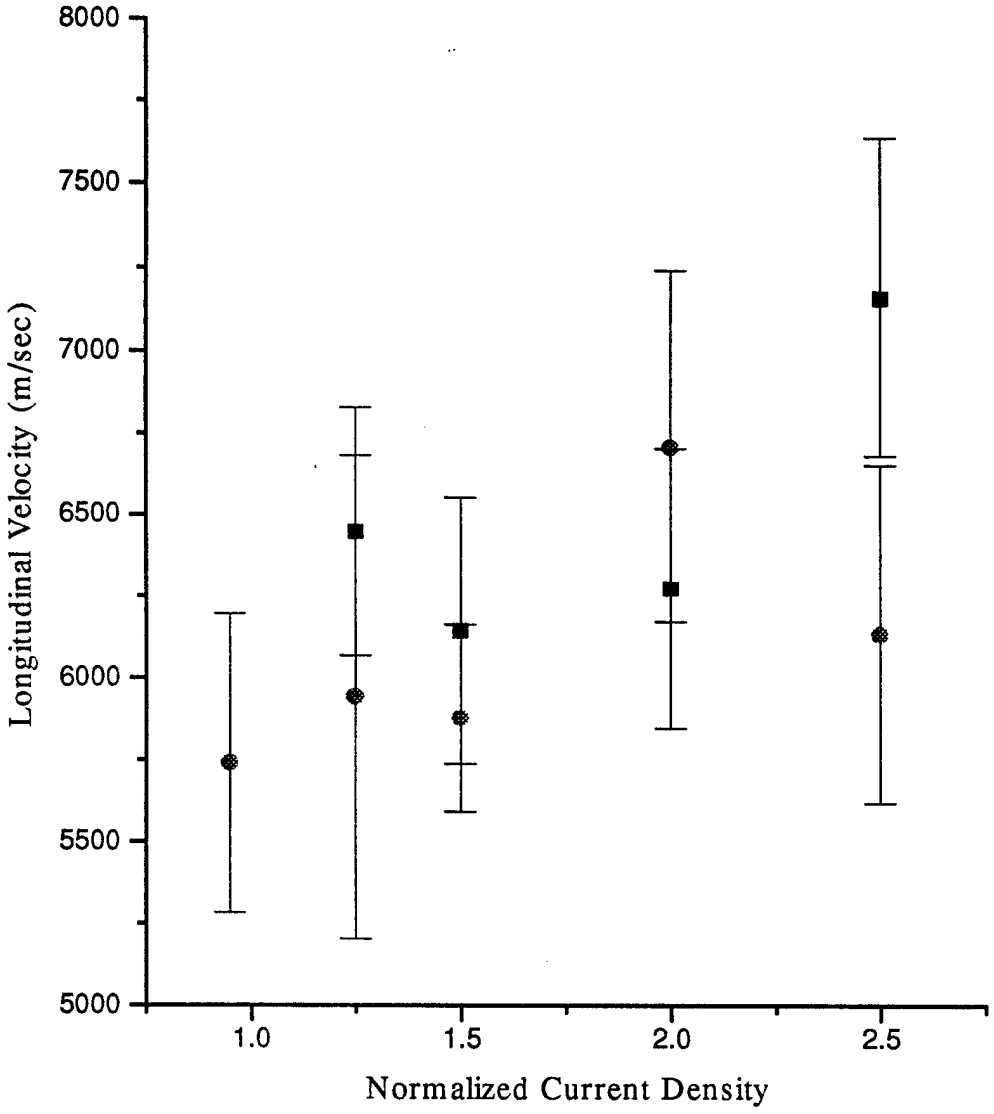

Figure 4 The measured longitudinal sound velocity of the chromium plotted as a function of normalized current density for two flow rates, ■ flow rate R1 and ● flow rate R2, respectively. Each point represents the average of the readings for all four locations on a ring and the bars represent the range in values for each ring.

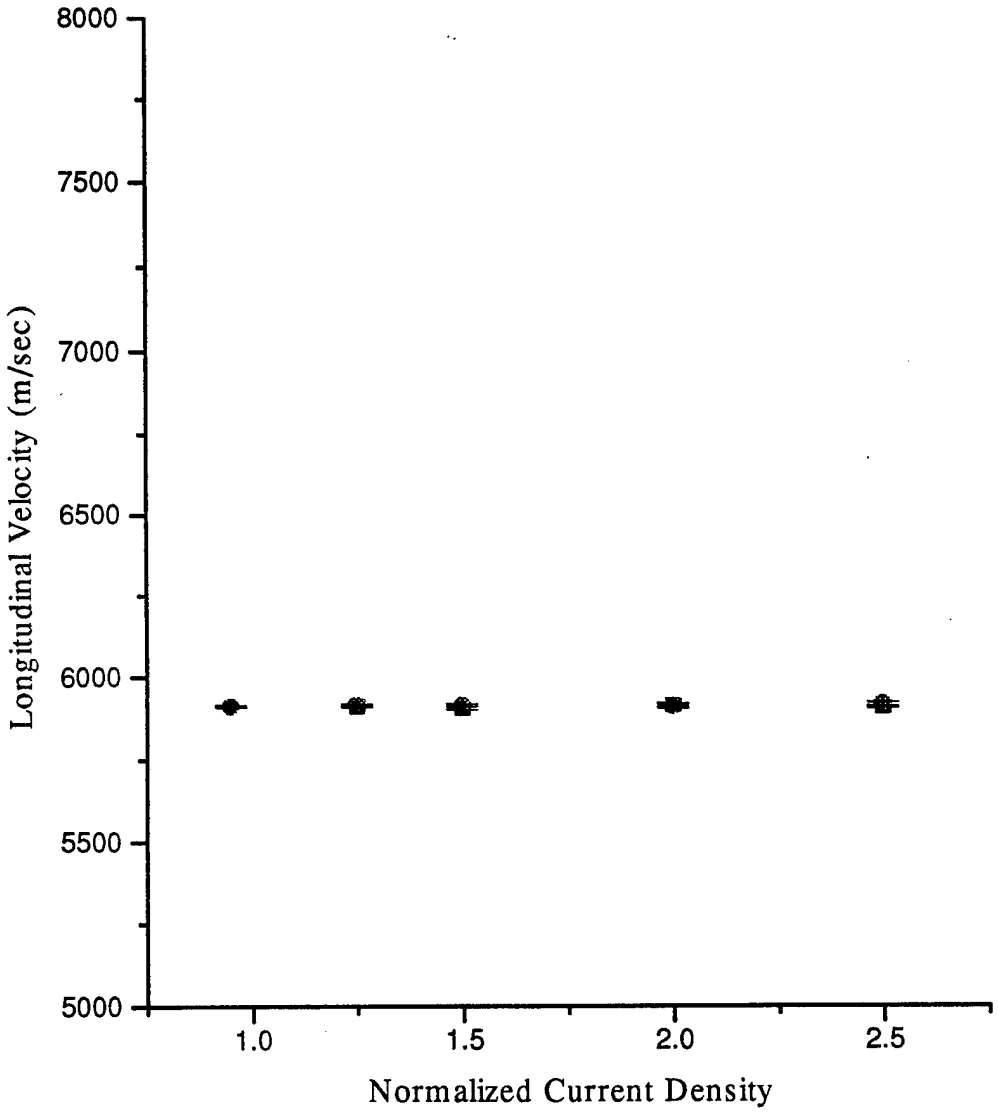

Figure 5 The measured longitudinal sound velocity of the steel plotted as a function of normalized current density for two flow rates, ■ flow rate R1 and ● flow rate R2, respectively. Each point represents the average of the readings for all four locations on a ring and the bars represent the range in values for each ring.

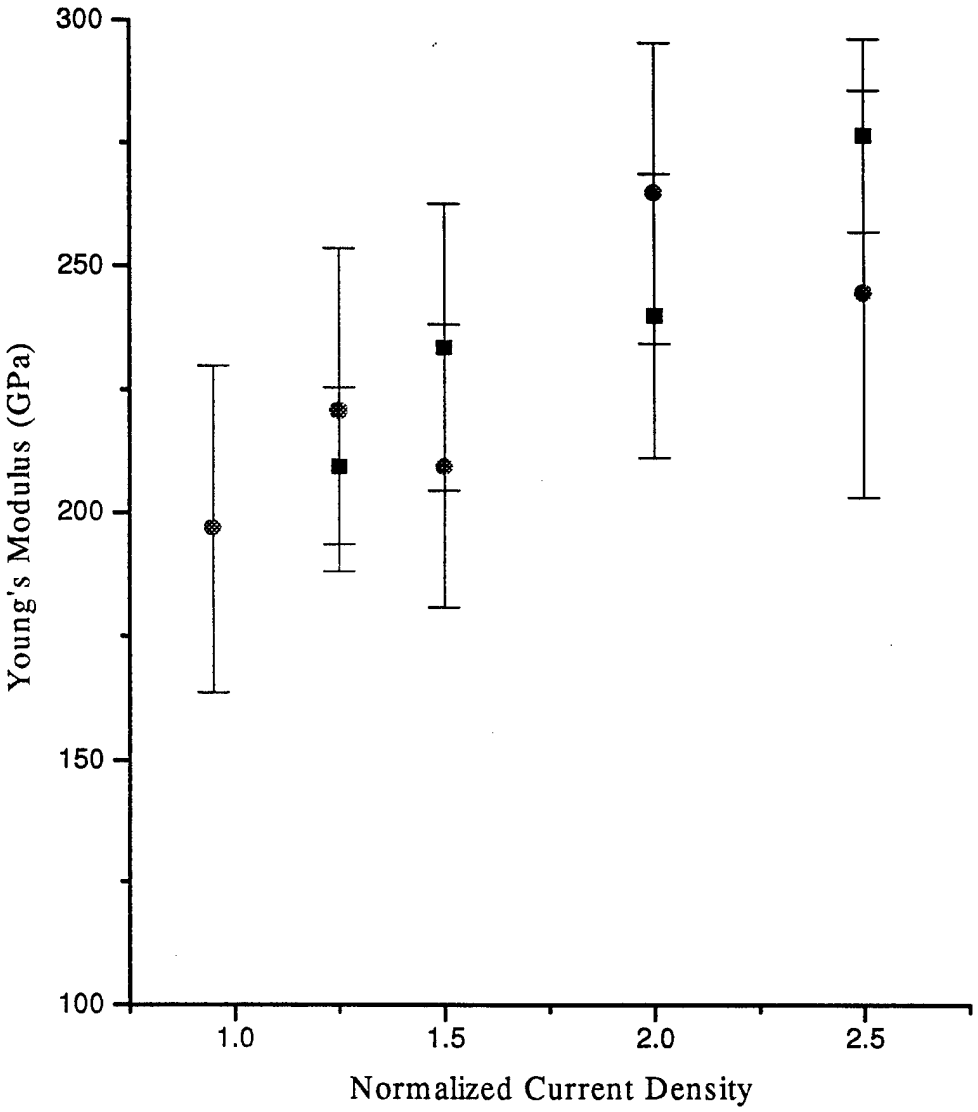

Figure 6 The calculated value of the Young's modulus of the chromium plotted as a function of normalized current density for two flow rates, ■ flow rate R1 and ● flow rate R2, respectively. Each point represents the average of the readings for all four locations on a ring and the bars represent the range in values for each ring. The moduli were calculated from the ultrasonic velocity measurements.

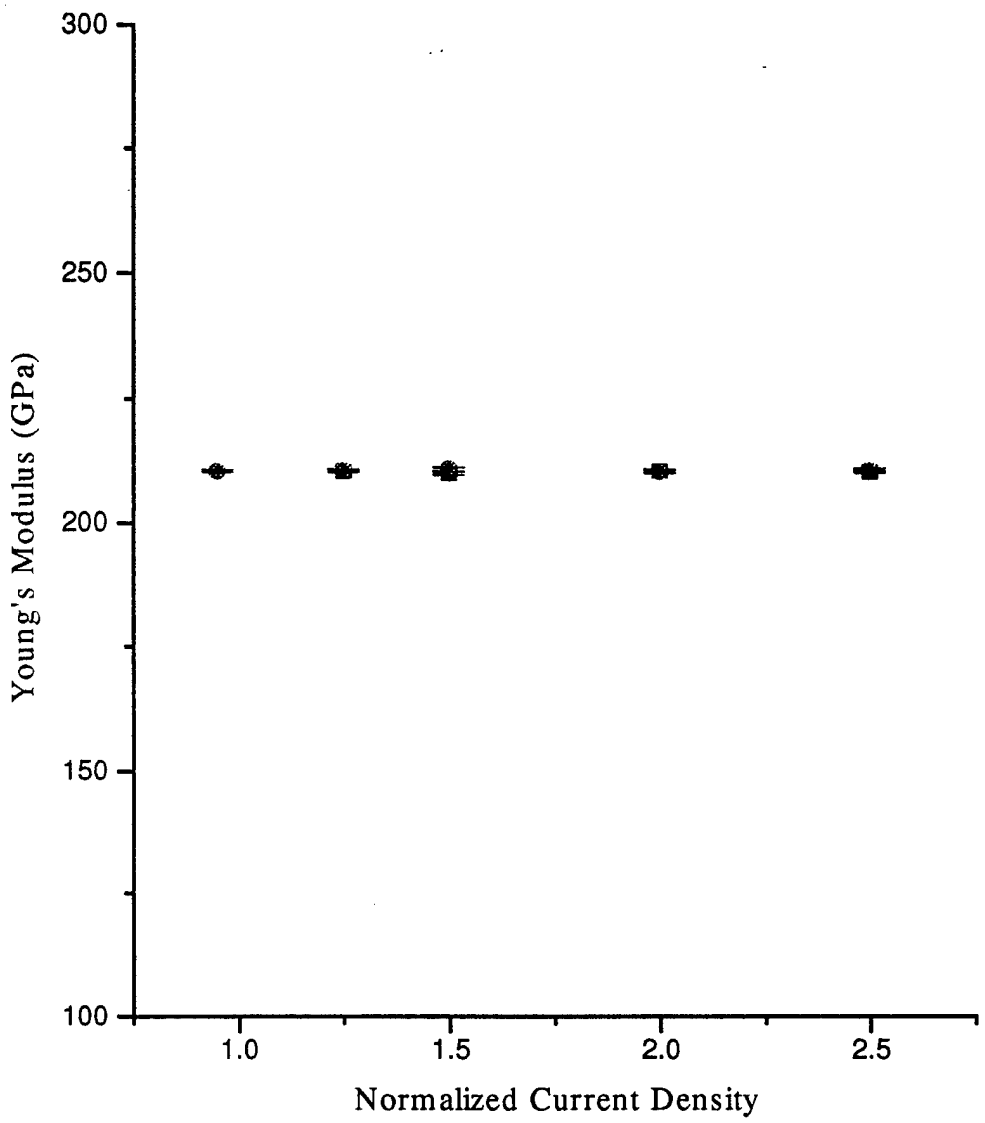

Figure 7 The calculated value of the Young's modulus of the steel plotted as a function of normalized current density for two flow rates, ■ flow rate R1 and ● flow rate R2, respectively. Each point represents the average of the readings for all four locations on a ring and the bars represent the range in values for each ring. The moduli were calculated from the ultrasonic velocity measurements.

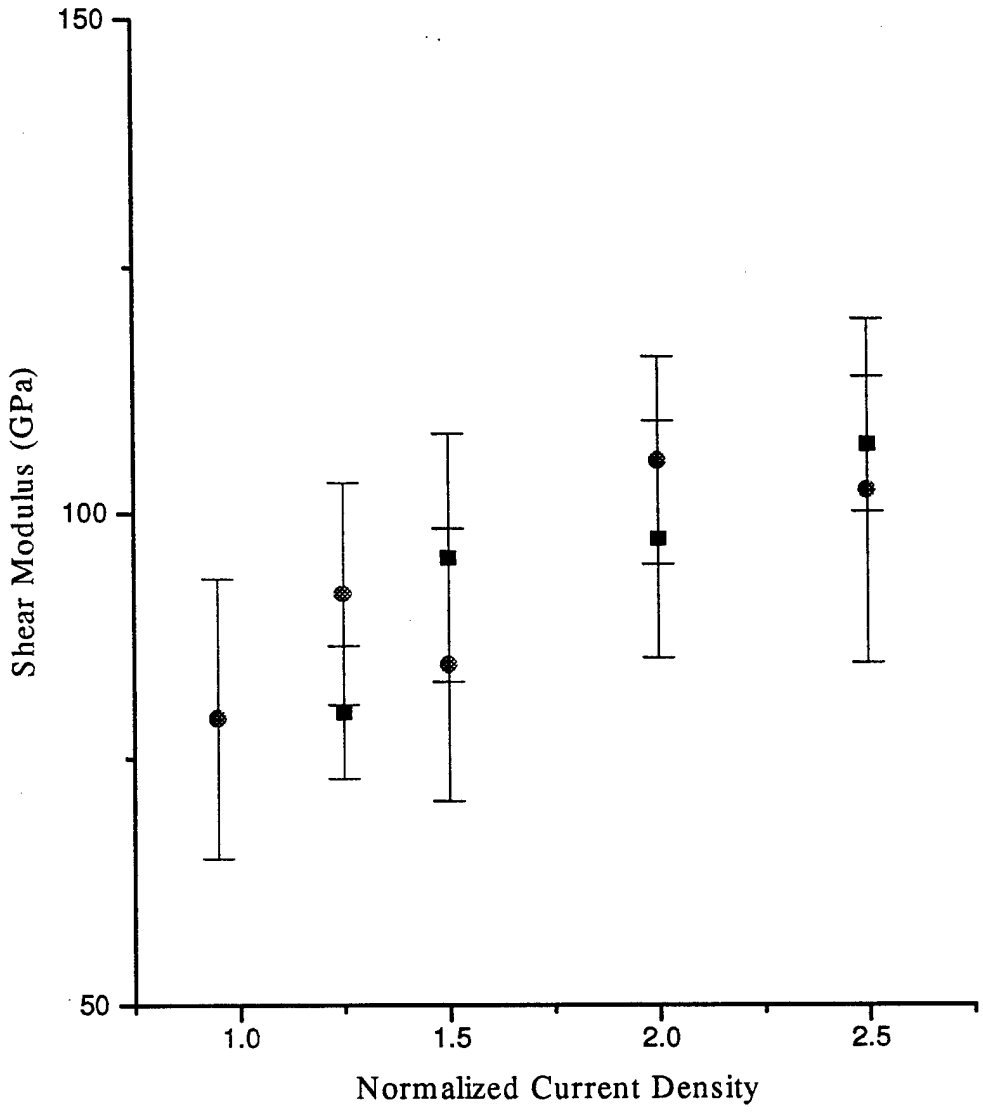

Figure 8 The calculated value of the shear modulus of the chromium plotted as a function of normalized current density for two flow rates, ■ flow rate R1 and ● flow rate R2, respectively. Each point represents the average of the readings for all four locations on a ring and the bars represent the range in values for each ring. The moduli were calculated from the ultrasonic velocity measurements.

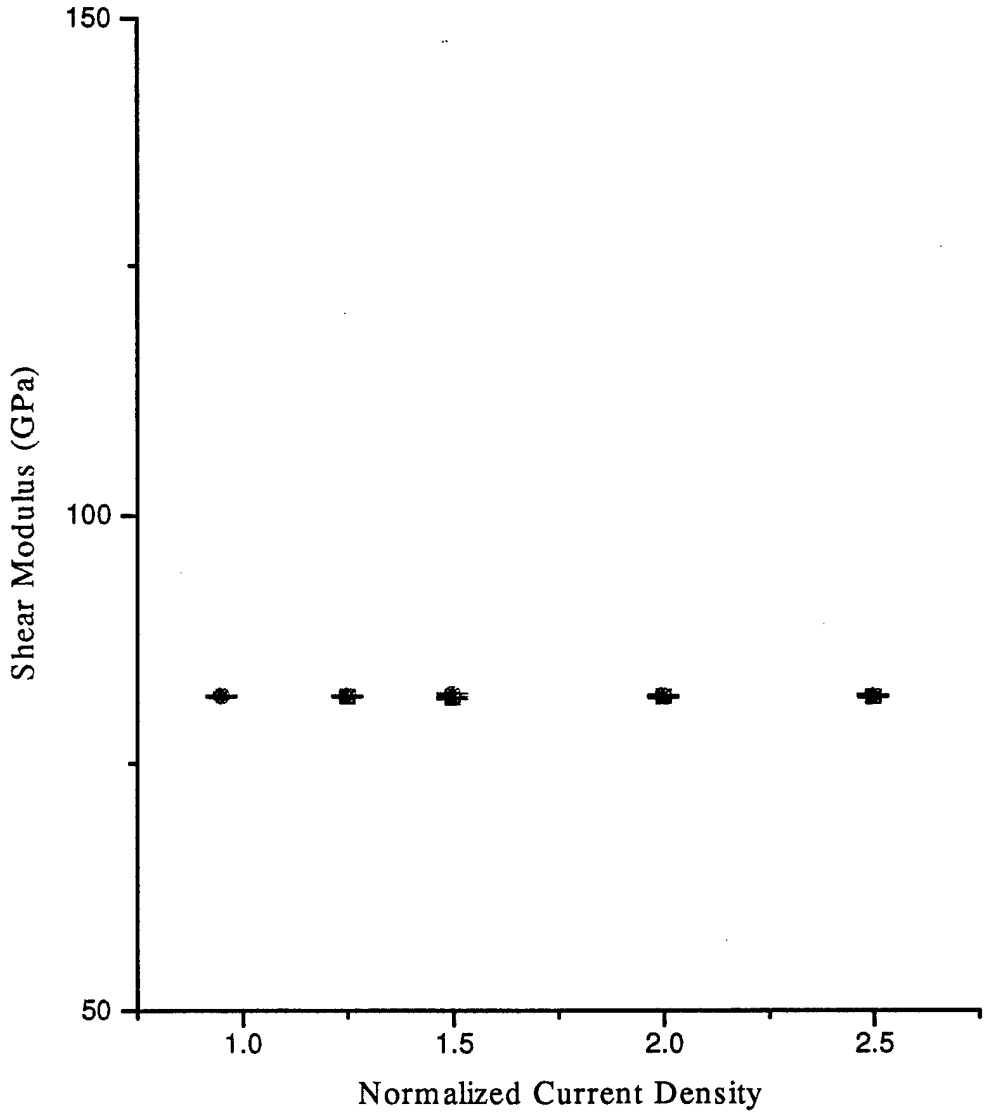

Figure 9 The calculated value of the shear modulus of the steel plotted as a function of normalized current density for two flow rates, ■ flow rate R1 and ● flow rate R2, respectively. Each point represents the average of the readings for all four locations on a ring and the bars represent the range in values for each ring. The moduli were calculated from the ultrasonic velocity measurements.

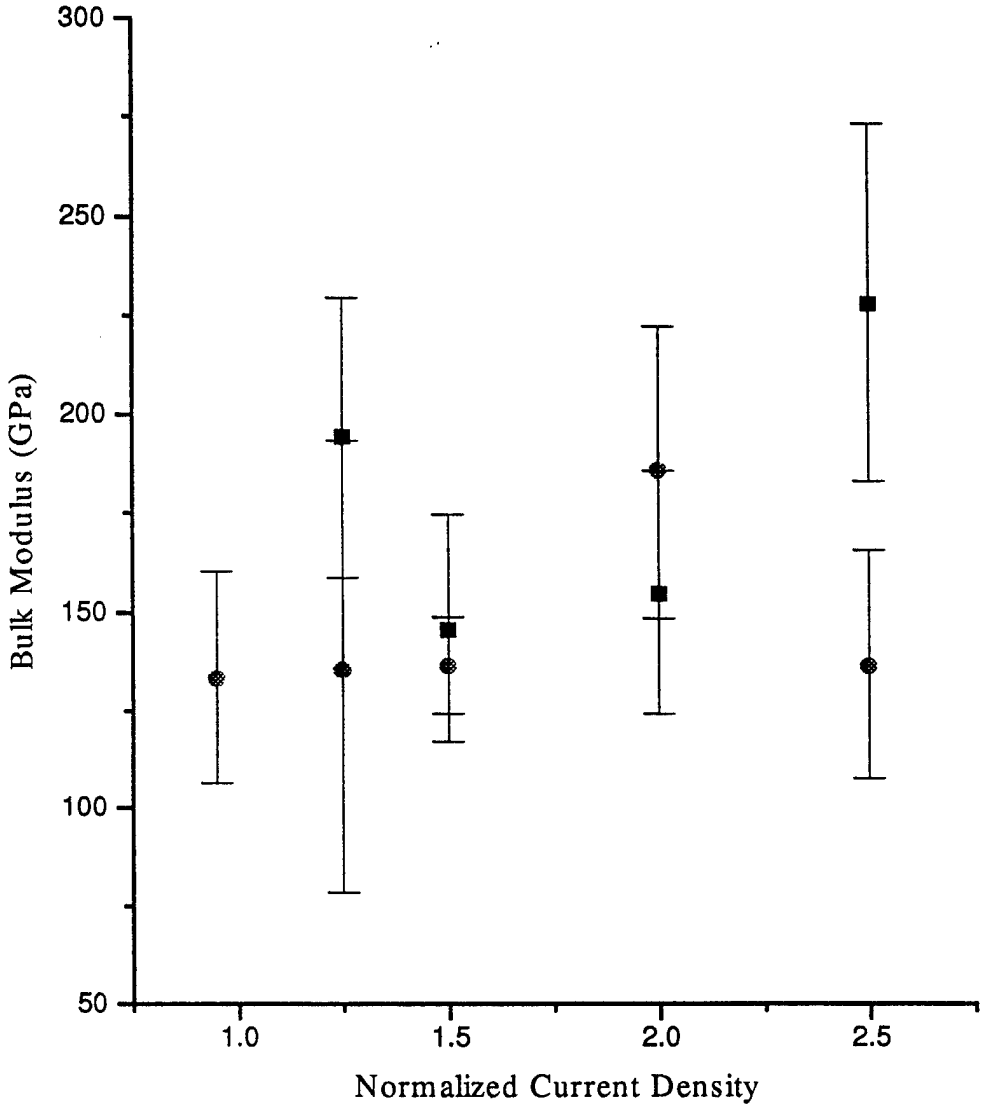

Figure 10 The calculated value of the bulk modulus of the chromium plotted as a function of normalized current density for two flow rates, ■ flow rate R1 and ● flow rate R2, respectively. Each point represents the average of the readings for all four locations on a ring and the bars represent the range in values for each ring. The moduli were calculated from the ultrasonic velocity measurements.

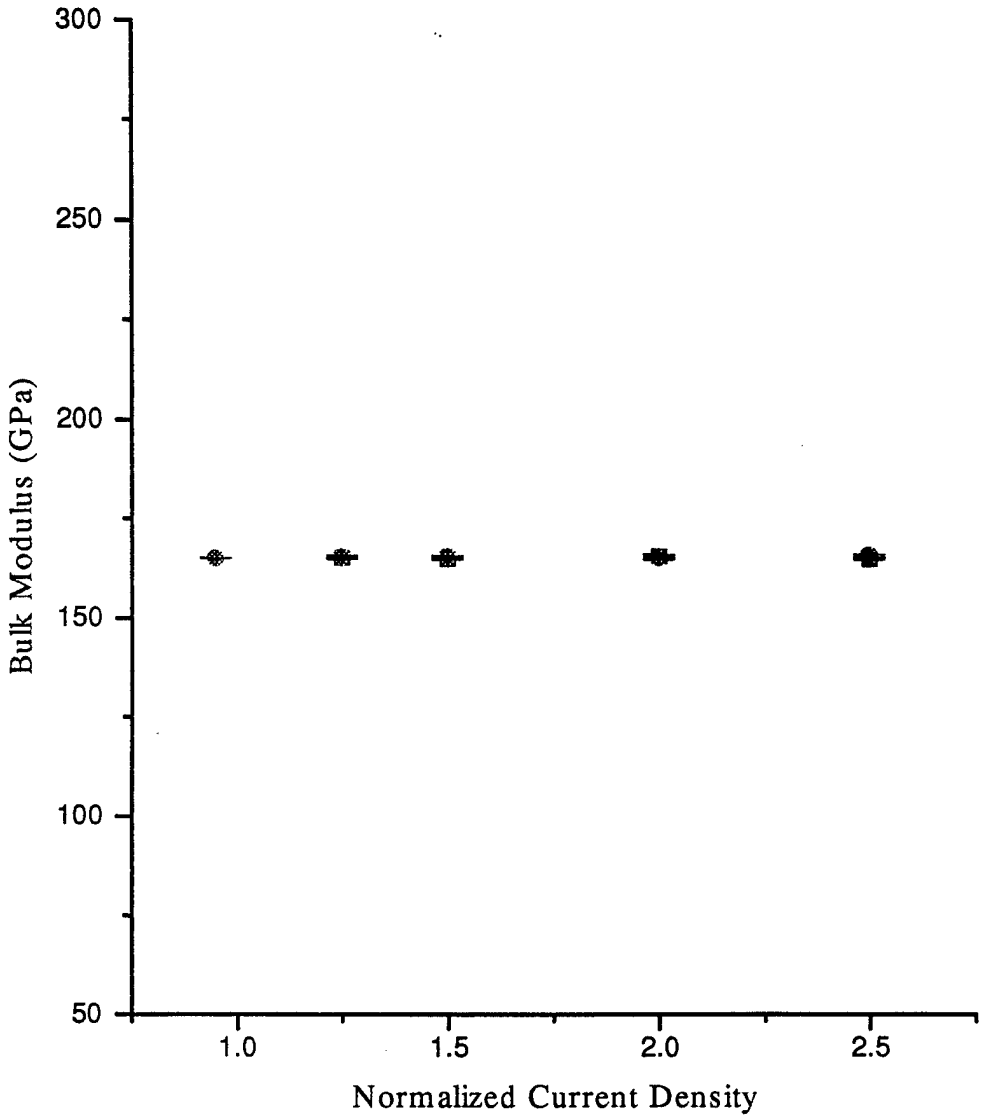

Figure 11 The calculated value of the bulk modulus of the steel plotted as a function of normalized current density for two flow rates, ■ flow rate R1 and ● flow rate R2, respectively. Each point represents the average of the readings for all four locations on a ring and the bars represent the range in values for each ring. The moduli were calculated from the ultrasonic velocity measurements.

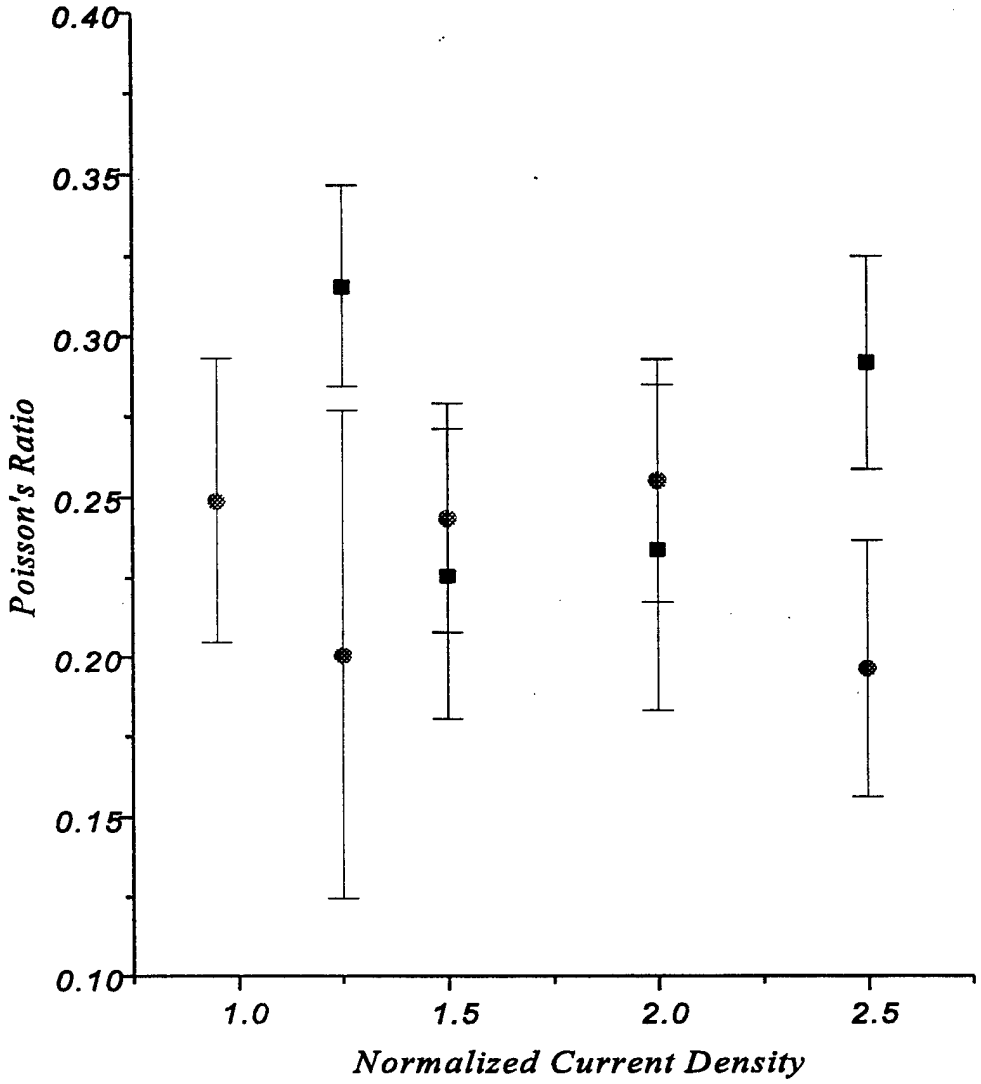

Figure 12 The calculated value of the Poisson's ratio of the chromium plotted as a function of normalized current density for two flow rates, ■ flow rate R1 and ● flow rate R2, respectively. Each point represents the average of the readings for all four locations on a ring and the bars represent the range in values for each ring. The Poisson's ratios were calculated from the ultrasonic velocity measurements.

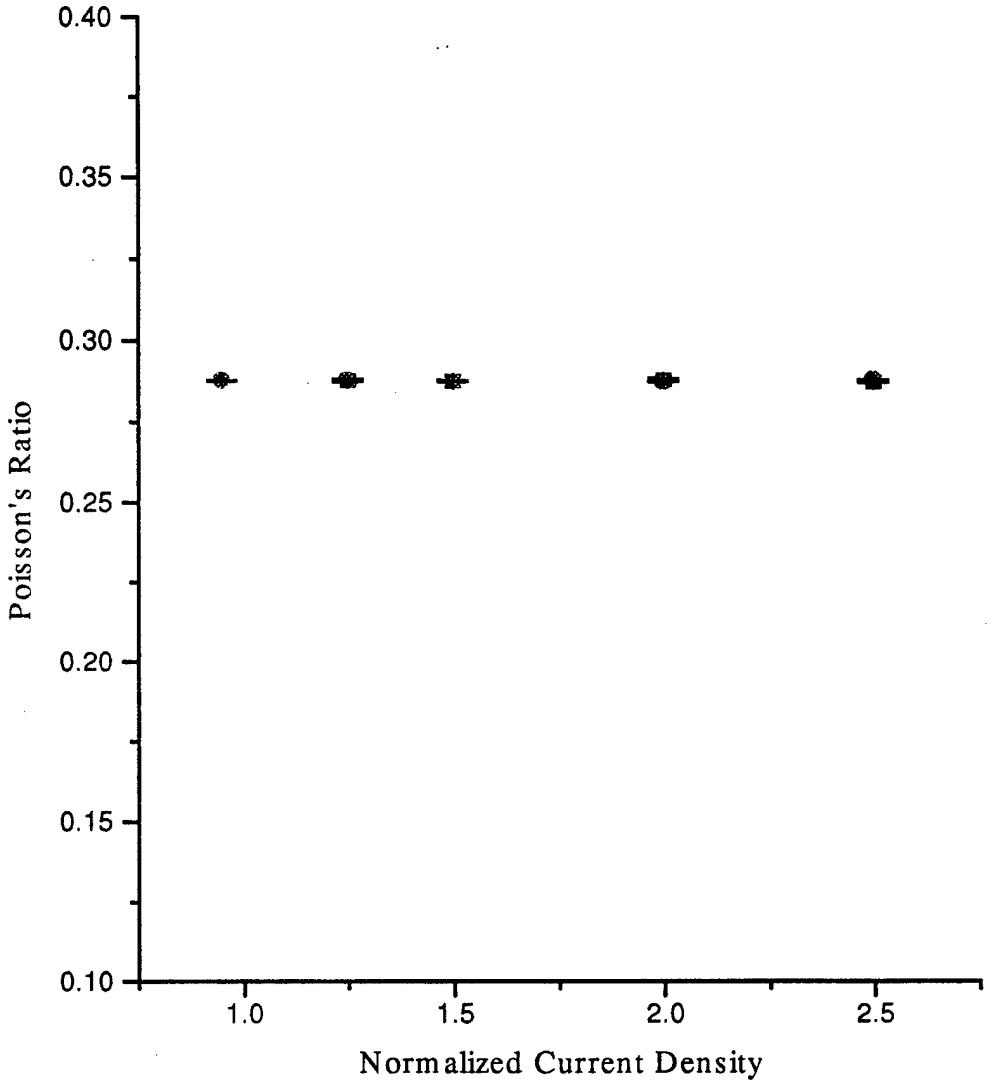

Figure 13 The calculated value of the Poisson's ratio of the steel plotted as a function of normalized current density for two flow rates, ■ flow rate R1 and ● flow rate R2, respectively. Each point represents the average of the readings for all four locations on a ring and the bars represent the range in values for each ring. The Poisson's ratios were calculated from the ultrasonic velocity measurements.

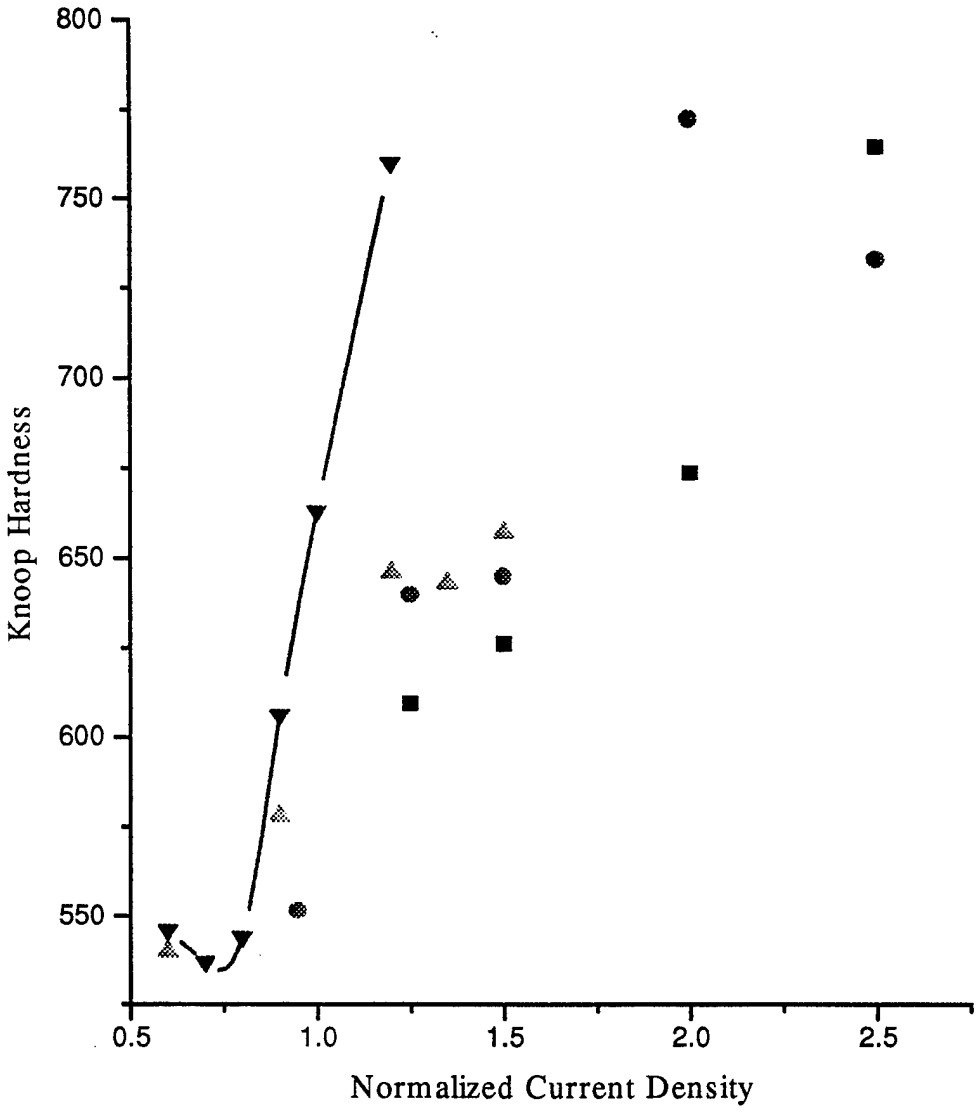

Figure 14 Knoop hardness data on chromium obtained in the present report in the shop VPF using the flow-through method at flow rate of R1 (■) and R2 (●) and for plates done in the laboratory in beakers from reports by Chen[3] (▲) and Pan et al[4] (▼), all plotted as a function of normalized current density.

TECHNICAL REPORT INTERNAL DISTRIBUTION LIST

	NO. OF COPIES
CHIEF, DEVELOPMENT ENGINEERING DIVISION	
ATTN: AMSTA-AR-CCB-DA	1
-DB	1
-DC	1
-DD	1
-DE	1
CHIEF, ENGINEERING DIVISION	
ATTN: AMSTA-AR-CCB-E	1
-EA	1
-EB	1
-EC	1
CHIEF, TECHNOLOGY DIVISION	
ATTN: AMSTA-AR-CCB-T	2
-TA	1
-TB	1
-TC	1
TECHNICAL LIBRARY	
ATTN: AMSTA-AR-CCB-O	5
TECHNICAL PUBLICATIONS & EDITING SECTION	
ATTN: AMSTA-AR-CCB-O	3
OPERATIONS DIRECTORATE	
ATTN: SIOWV-ODP-P	1
DIRECTOR, PROCUREMENT & CONTRACTING DIRECTORATE	
ATTN: SIOWV-PP	1
DIRECTOR, PRODUCT ASSURANCE & TEST DIRECTORATE	
ATTN: SIOWV-QA	1

NOTE: PLEASE NOTIFY DIRECTOR, BENÉT LABORATORIES, ATTN: AMSTA-AR-CCB-O OF ADDRESS CHANGES.

TECHNICAL REPORT EXTERNAL DISTRIBUTION LIST

	NO. OF COPIES
ASST SEC OF THE ARMY RESEARCH AND DEVELOPMENT ATTN: DEPT FOR SCI AND TECH THE PENTAGON WASHINGTON, D.C. 20310-0103	1
DEFENSE TECHNICAL INFO CENTER ATTN: DTIC-OCP (ACQUISITIONS) 8725 JOHN J. KINGMAN ROAD STE 0944 FT. BELVOIR, VA 22060-6218	2
COMMANDER U.S. ARMY ARDEC ATTN: AMSTA-AR-AEE, BLDG. 3022 AMSTA-AR-AES, BLDG. 321 AMSTA-AR-AET-O, BLDG. 183 AMSTA-AR-FSA, BLDG. 354 AMSTA-AR-FSM-E AMSTA-AR-FSS-D, BLDG. 94 AMSTA-AR-IMC, BLDG. 59 PICATINNY ARSENAL, NJ 07806-5000	 1 1 1 1 1 1 2
DIRECTOR U.S. ARMY RESEARCH LABORATORY ATTN: AMSRL-DD-T, BLDG. 305 ABERDEEN PROVING GROUND, MD 21005-5066	1
DIRECTOR U.S. ARMY RESEARCH LABORATORY ATTN: AMSRL-WT-PD (DR. B. BURNS) ABERDEEN PROVING GROUND, MD 21005-5066	1
DIRECTOR U.S. MATERIEL SYSTEMS ANALYSIS ACTV ATTN: AMXSY-MP ABERDEEN PROVING GROUND, MD 21005-5071	1
COMMANDER ROCK ISLAND ARSENAL ATTN: SMCRI-SEM ROCK ISLAND, IL 61299-5001	1
MIAC/CINDAS PURDUE UNIVERSITY 2595 YEAGER ROAD WEST LAFAYETTE, IN 47906-1398	1
COMMANDER U.S. ARMY TANK-AUTMV R&D COMMAND ATTN: AMSTA-DDL (TECH LIBRARY) WARREN, MI 48397-5000	1
COMMANDER U.S. MILITARY ACADEMY ATTN: DEPARTMENT OF MECHANICS WEST POINT, NY 10966-1792	1
U.S. ARMY MISSILE COMMAND REDSTONE SCIENTIFIC INFO CENTER ATTN: AMSMI-RD-CS-R/DOCUMENTS BLDG. 4484 REDSTONE ARSENAL, AL 35898-5241	2
COMMANDER U.S. ARMY FOREIGN SCI & TECH CENTER ATTN: DRXST-SD 220 7TH STREET, N.E. CHARLOTTESVILLE, VA 22901	1
COMMANDER U.S. ARMY LABCOM, ISA ATTN: SLCIS-IM-TL 2800 POWER MILL ROAD ADELPHI, MD 20783-1145	1

NOTE: PLEASE NOTIFY COMMANDER, ARMAMENT RESEARCH, DEVELOPMENT, AND ENGINEERING CENTER, BENÉT LABORATORIES, CCAC, U.S. ARMY TANK-AUTOMOTIVE AND ARMAMENTS COMMAND, AMSTA-AR-CCB-O, WATERVLIET, NY 12189-4050 OF ADDRESS CHANGES.

TECHNICAL REPORT EXTERNAL DISTRIBUTION LIST (CONT'D)

	NO. OF COPIES
COMMANDER U.S. ARMY RESEARCH OFFICE ATTN: CHIEF, IPO P.O. BOX 12211 RESEARCH TRIANGLE PARK, NC 27709-2211	1
DIRECTOR U.S. NAVAL RESEARCH LABORATORY ATTN: MATERIALS SCI & TECH DIV WASHINGTON, D.C. 20375	1
WRIGHT LABORATORY ARMAMENT DIRECTORATE ATTN: WL/MNM EGLIN AFB, FL 32542-6810	1
WRIGHT LABORATORY ARMAMENT DIRECTORATE ATTN: WL/MNMF EGLIN AFB, FL 32542-6810	1

NOTE: PLEASE NOTIFY COMMANDER, ARMAMENT RESEARCH, DEVELOPMENT, AND ENGINEERING CENTER, BENÉT LABORATORIES, CCAC, U.S. ARMY TANK-AUTOMOTIVE AND ARMAMENTS COMMAND, AMSTA-AR-CCB-O, WATERVLIET, NY 12189-4050 OF ADDRESS CHANGES.